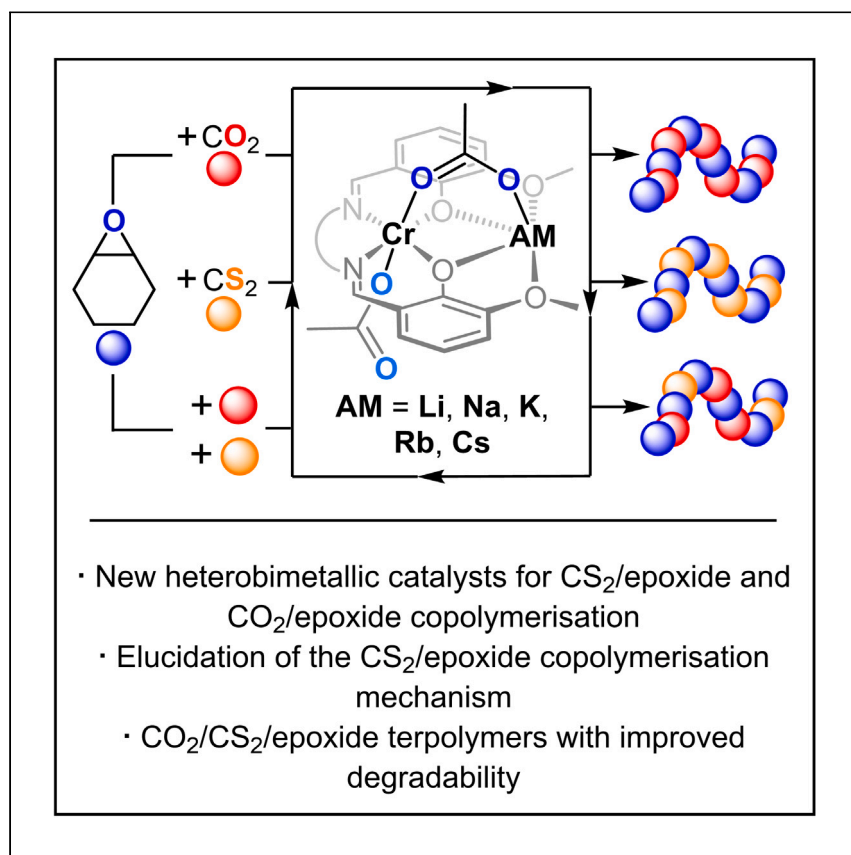


Article

# Mechanistic mapping of (CS<sub>2</sub>/CO<sub>2</sub>)/epoxide copolymerization catalysis leads to terpolymers with improved degradability



Here, Stephan et al. report how carbon dioxide and carbon disulfide copolymerization relate to each other. Ultimately, their findings demonstrate that controlling the incorporation of sulfur-containing links into polycarbonates improves degradability.

Jenny Stephan, Merlin R. Stühler, Susanne M. Rupf, Sam Neale, Alex J. Plajer

sen36@bath.ac.uk (S.N.)  
plajer@zedat.fu-berlin.de (A.J.P.)

Highlights

Systematic study comparing CS<sub>2</sub> and CO<sub>2</sub> epoxide copolymerization

Elucidation of oxygen/sulfur scrambling mechanism is performed

Incorporation of sulfur centers into polycarbonates improves degradability of terpolymers

## Article

Mechanistic mapping of (CS<sub>2</sub>/CO<sub>2</sub>)/epoxide copolymerization catalysis leads to terpolymers with improved degradabilityJenny Stephan,<sup>1</sup> Merlin R. Stühler,<sup>1</sup> Susanne M. Rupf,<sup>1</sup> Sam Neale,<sup>2,\*</sup> and Alex J. Plajer<sup>1,3,4,\*</sup>

## SUMMARY

The placement of main-group functionalities within polymers represents a strategy to access a wide catalog of materials but is limited by poor understanding of the catalyst selection criteria and polymerization mechanism when moving down the periodic table. Here, we study a series of new heterobimetallic carbon dioxide and carbon disulfide/epoxide copolymerization catalysts that allow for a comparative mechanistic understanding of two ring-opening copolymerization processes. We reveal that the distinct roles each metal plays are preserved from carbon dioxide to carbon disulfide, maintaining activity and selectivity across copolymerizations. Experimental and computational studies show that carbon disulfide/epoxide copolymerization can be understood as a series of structurally related insertion events that are interlinked by a central oxygen/sulfur scrambling reaction at the propagating chain end. This facilitates the synthesis of new carbon dioxide-/carbon disulfide-/epoxide-derived terpolymers with improved degradability over the parent carbon dioxide/epoxide copolymers at low levels of sulfur incorporation.

## INTRODUCTION

The incorporation of heteroatoms into the polymer backbone renders these more susceptible to degradation via physical, chemical, and biochemical pathways and even facilitates new chemical recycling methods.<sup>1–8</sup> One increasingly popular methodology to achieve their synthesis is the alternating ring-opening copolymerization (ROCOP) of heteroallenes with heterocycles, which allows, for example, the synthesis of sustainable polycarbonates from globally accumulating waste CO<sub>2</sub>.<sup>9–17</sup> Also accessible are sulfur-containing analogs such as polythiocarbonate from the ROCOP of CS<sub>2</sub>, a monomer that can be directly sourced from elemental sulfur, which is likewise a waste product of the petrochemical industry.<sup>18–33</sup> Investigation of these ROCOPs is furthermore relevant to elucidate how periodic trends affect polymerization mechanisms and to enable the design of more complex terpolymerization processes in combination with CO<sub>2</sub>, which could impart the chemical properties of sulfur onto CO<sub>2</sub>-derived polycarbonates. However, compared with CO<sub>2</sub>/epoxide ROCOP, significantly less is known about CS<sub>2</sub>/epoxide ROCOP, and moreover, CO<sub>2</sub>/CS<sub>2</sub>/epoxide is entirely unknown.<sup>34–40</sup> This is perhaps due to the complexity of the copolymerization process yielding polymers comprising dithiocarbonate –O–C(=S)–S– (OSS) links from alternating epoxide and CS<sub>2</sub> insertion as well as other (thio)carbonate links (–O–C(=O)–S– OOS, –O–C(=S)–O– OSO, –S–C(=S)–S– SSS, –O–C(=O)–O– OOO) (Figure 1). This observation has been termed O/S scrambling and is strongly dependent on reaction conditions as well as catalyst selection. In this regard, the groups of Wan,

<sup>1</sup>Institut für Chemie und Biochemie, Freie Universität Berlin, Fabeckstraße 34–36, 14195 Berlin, Germany

<sup>2</sup>Department of Chemistry, University of Bath, Claverton Down, Bath BA2 7AY, UK

<sup>3</sup>Twitter: @ajplajer

<sup>4</sup>Lead contact

\*Correspondence: sen36@bath.ac.uk (S.N.), plajer@zedat.fu-berlin.de (A.J.P.)

<https://doi.org/10.1016/j.xcrp.2023.101510>



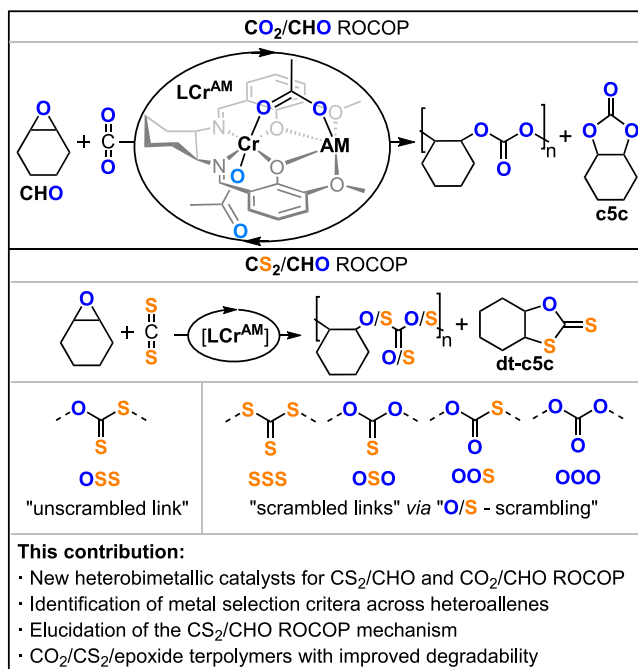


**Figure 1. Outline of the study**

Comparison of products formed during (CS<sub>2</sub>/CO<sub>2</sub>)/CHO ROCOPs. Abbreviations: AM, alkali metal (Li, Na, K, Rb, Cs); CHO, cyclohexene oxide; c5c, cyclic five-membered carbonate; dt-c5c, cyclic five-membered dithiocarbonate; [R<sub>n</sub>], polymer chain.

Zhang, Darensbourg, and Werner assigned the products generated by CS<sub>2</sub> ROCOP and formulated different mechanistic hypotheses explaining the formation of these.<sup>35,36,38,39</sup> However, the suggested reaction mechanisms differ considerably (i.e., scrambling induced by nucleophilic attack of chain ends or polymer links by residual monomers, halide cocatalysts, or alkoxide chain ends), and further experimental and computational support is required to elucidate the process, as most suggested pathways remain mere hypotheses. In CO<sub>2</sub> ROCOP, one of the most promising catalyst design concepts is heterobimetallic cooperativity, which allows for the improvement of activity beyond values achievable for homomultinuclear metal or multicomponent catalysts.<sup>41,42</sup> These catalysts are often synthetically very accessible, and in particular, Williams and co-workers presented a series of well-performing catalysts based on vanillin-derived ligands (similar to H<sub>2</sub>L; Figure 2) for all-oxygen ROCOP.<sup>43–46</sup> Furthermore, heterobimetallic catalysts in general maintain activity at low CO<sub>2</sub> pressure as well as high dilution, the latter being attractive for CS<sub>2</sub>/epoxide ROCOP requiring an excess of liquid CS<sub>2</sub>. However, it is unclear whether heterobimetallic cooperativity is transferrable from O- to S-containing monomers and to what extent catalyst selection criteria and the ROCOP mechanism itself are affected by periodic trends. In a recent study, we found that a heterobimetallic Cr(III)K catalyst featuring a macrocyclic ligand enables the selective copolymerization of CS<sub>2</sub> and oxetanes to poly(dithiocarbonates) and also showed excellent sequence selectivity in CS<sub>2</sub>/cyclohexene oxide (CHO) ROCOP.<sup>47</sup> However, we were unable to prepare the Li and Cs derivatives of the complex, preventing the investigation of a complete series of Cr(III)AM (AM = alkali metal) catalysts. Furthermore, no comparative CO<sub>2</sub> co- and terpolymerizations or elucidations of the CS<sub>2</sub> ROCOP reaction mechanism could be presented. Nevertheless, this inspired us to survey related catalysts in an attempt to answer the open mechanistic questions stated above, which we report in this contribution.

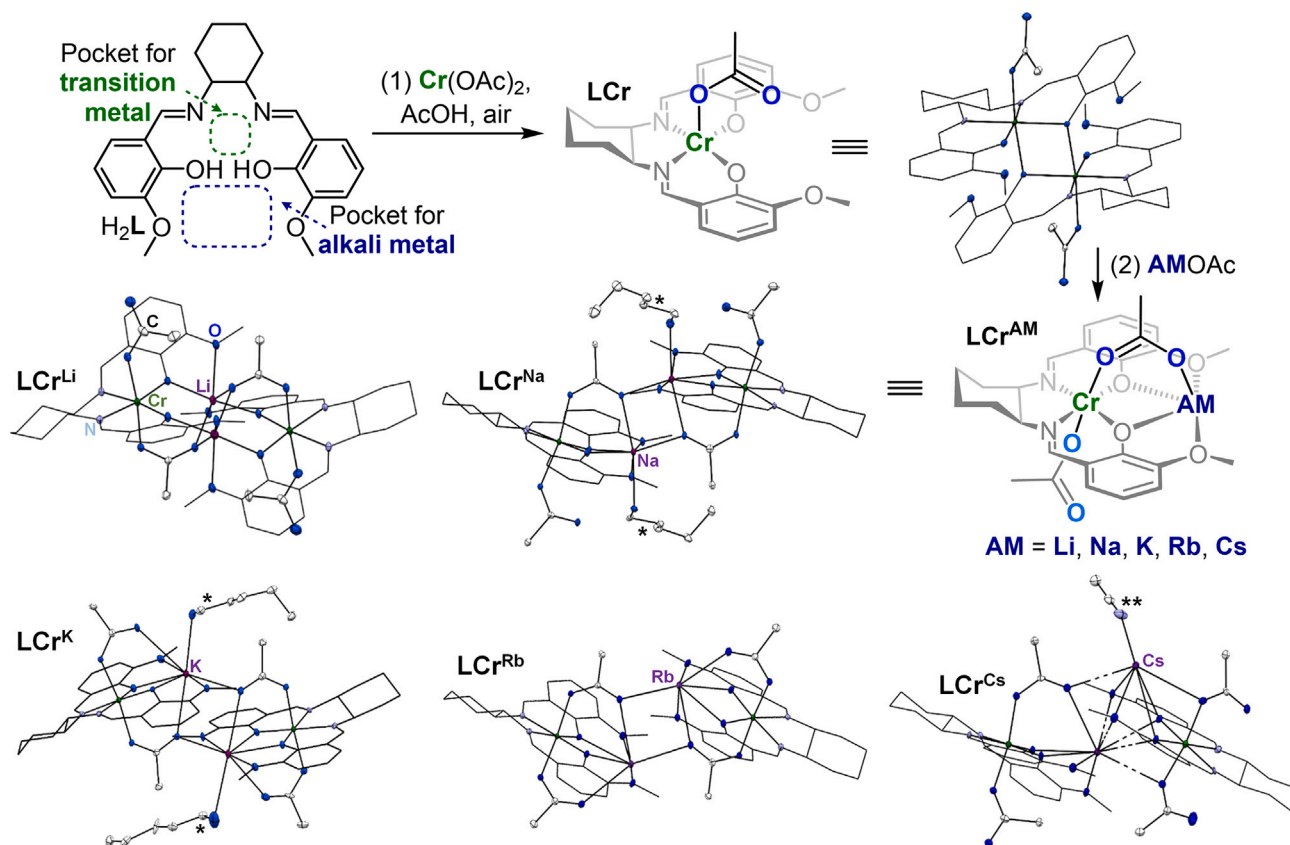


**Figure 2. Family of copolymerization catalysts**

Synthesis and molecular structures in the solid state of new  $LM^{AM}$  catalysts presented in this study. Hydrogen atoms and disorder omitted for clarity; thermal ellipsoids displayed at 20%–30% probability; color code: green, Cr; purple, alkali metal; dark blue, O; bright blue, N; white, C. \*coordinated butanol and \*\*coordinated acetonitrile from crystallization solvent.

## RESULTS AND DISCUSSION

### Catalyst synthesis and characterization

Motivated by the precedence for catalysts comprising Cr(III) in  $CX_2$ /epoxide ROCOP ( $X = O, S$ ), a series of heterobimetallic Cr(III)AM (AM = Li, Na, K, Rb, Cs) complexes was targeted based on the heterobinucleating ligand  $H_2L$  (Note S2).<sup>40,45</sup> Treatment of  $H_2L$  with  $Cr(OAc)_2$  following aerobic oxidation in the presence of HOAc yields LCr, which can be easily coordinated to the AM acetates by reaction with AMOAc (AM = Li, Na, K, Rb, Cs) forming  $LCr^{AM}$ , which were characterized using single-crystal X-ray diffraction (XRD), high-resolution electrospray ionization mass spectrometry (HR-ESIMS), UV-visible (UV-vis), and elemental analysis. As shown in Figure 2, the complexes form dimeric arrangements in the solid state with different bridging modes depending on the AM. However, all complexes feature six-coordinate chromate centers through equatorial coordination of the N,N,O,O donors and axial coordination through two acetate oxygens. Also,  $LCr^{Na/K/Cs}$  show donor solvent coordination at the AM.  $LCr^{Na}$ ,  $LCr^K$ , and  $LCr^{Rb}$  exhibit AM coordination via all four half-crown donor oxygens of one ligand scaffold. In  $LCr^{Li}$ , on the other hand, Li coordination occurs via one phenolate and one methoxy oxygen center from two different ligand scaffolds.  $LCr^{Cs}$  forms a double-decker-type arrangement in which one Cs is sandwiched between two half-crown units, while another Cs face caps one side of the dimer.

**Table 1. CO<sub>2</sub>/CHO and CS<sub>2</sub>/CHO ROCOP employing the LM<sup>AM</sup>**

Cat.	CO <sub>2</sub> run <sup>a</sup>	TON <sup>b</sup>	TOF (h <sup>-1</sup> ) <sup>c</sup>	Pol. (%) <sup>d</sup>	Link. (%) <sup>e</sup>	M <sub>n</sub> (kDa) (Đ) <sup>f</sup>	CS <sub>2</sub> run <sup>g</sup>	TON <sup>b</sup>	TOF (h <sup>-1</sup> ) <sup>h</sup>	Pol. (%) <sup>i</sup>	OSS (%) <sup>j</sup>	M <sub>n</sub> (kDa) (Đ) <sup>f</sup>
LCr <sup>Li</sup>	#1	322	30 ± 2	95	76	6.3 (1.2)	#7	110	<5	12	>1	ND
LCr <sup>Na</sup>	#2	439	75 ± 2	99	99	14.8 (1.3)	#8	251	11 ± 2	61	5	5.4 (1.3)
LCr <sup>K</sup>	#3	662	127 ± 4	99	98	15.8 (1.4)	#9	845	112 ± 12	76	37	15.6 (1.5)
LCr <sup>Rb</sup>	#4	623	112 ± 4	99	99	13.0 (1.3)	#10	866	67 ± 2	76	53	12.4 (1.7)
LCr <sup>Cs</sup>	#5	576	157 ± 8	99	99	14.4 (1.5)	#11	870	144 ± 10	76	58	14.4 (1.6)
LCr <sup>Rb</sup>	#6 <sup>k</sup>	493	443 ± 30	99	92	10.9 (1.2)	#12 <sup>l</sup>	685	591 ± 32	35	16	4.9 (1.6)

<sup>a</sup>Copolymerization at 1 equiv. LM<sup>AM</sup>: 1,000 equiv CHO, 4 bar CO<sub>2</sub>, T = 100°C; reaction stopped after 24 h or at viscosity limit when stirring ceased.

<sup>b</sup>Turnover number (TON), number of moles of CHO consumed per mole of catalyst.

<sup>c</sup>Turnover frequency (TOF) determined from initial rates analysis by <sup>1</sup>H NMR aliquot monitoring (typically 5%–30% conversion) as TON/time.

<sup>d</sup>Relative integrals in the normalized <sup>1</sup>H NMR spectrum of tertiary CH resonances due to polymer vs. c5c.

<sup>e</sup>Relative integrals in the normalized <sup>1</sup>H NMR spectrum of tertiary CH resonances due to carbonate vs. ether links.

<sup>f</sup>Determined by GPC (gel permeation chromatography) measurements conducted in THF, using narrow MW polystyrene standards to calibrate the instrument.

<sup>g</sup>Copolymerization at 1 equiv LM<sup>AM</sup>: 1,000 equiv CHO: 2,000 equiv CS<sub>2</sub>. T = 60°C. Turnover number (TON), number of moles of CHO/CHS coupled to hetero-carbonates per mole of catalyst.

<sup>h</sup>Turnover frequency (TOF) determined from rate analysis by <sup>1</sup>H NMR aliquot monitoring (linear region following the initiation period, typically between 10% and 40%) as TON/time.

<sup>i</sup>Relative integrals in the normalized <sup>1</sup>H NMR spectrum (CDCl<sub>3</sub>, 25°C, 400 MHz) of tertiary CH resonances due to polymeric relative to cyclic heterocarbonates.

<sup>j</sup>Relative integrals in the normalized <sup>1</sup>H NMR spectrum of tertiary CH resonances due to OSS vs. other heterocarbonate links.

<sup>k</sup>T = 120°C.

<sup>l</sup>T = 100°C.

### CO<sub>2</sub>/epoxide and CS<sub>2</sub>/epoxide ROCOP

With the LCr<sup>AM</sup> in hand, we turned toward the ROCOPs of CO<sub>2</sub> and CS<sub>2</sub> with the commonly employed benchmark epoxide CHO (Notes S3 and S4). CO<sub>2</sub>/CHO ROCOP was performed at a loading of 1 equiv LM<sup>AM</sup> to 1,000 equiv CHO, 100°C, and 4 bar CO<sub>2</sub> pressure and monitored by aliquot analysis via <sup>1</sup>H nuclear magnetic resonance (NMR) to accurately compare reaction kinetics and product distributions. In doing so, we found an increase in selectivity and activity when moving to heavier AMs (LCr<sup>Cs</sup> ≈ LCr<sup>K</sup> ≈ LCr<sup>Rb</sup> > LCr<sup>Na</sup> > LCr<sup>Li</sup>, with LCr<sup>Cs</sup> > LCr<sup>K</sup>) with turnover frequencies (TOFs) ranging from 30 to 157 h<sup>-1</sup> (Table 1, runs #1–5). All catalysts exhibit excellent polymer (i.e., <5% cyclic five-membered carbonate [c5c] production) and linkage selectivity (i.e., >99% carbonate vs. ether links), except for LCr<sup>Li</sup>, producing approximately 24% ether linkages resulting from epoxide homopropagation. The copolymerizations yield materials with bimodal molecular weights (M<sub>n</sub> = 6.3–14.4 kDa, Đ = 1.2–1.45) increasing with monomer conversions typically observed in CO<sub>2</sub>/CHO ROCOP. Increasing the reaction temperature results in higher TOFs of 443 h<sup>-1</sup> at 120°C and slightly decreases the polymer selectivity vs. c5c (Figure 2) to 92% (63% polymer selectivity at 140°C) due to entropically favored c5c generation. Having established LCr<sup>AM</sup> as active catalysts, we moved toward exploring CS<sub>2</sub>/CHO ROCOP, which was conducted at 60°C at a loading of 1 equiv LCr<sup>AM</sup>: 1,000 equiv CHO: 2,000 equiv CS<sub>2</sub>. As can be seen in the NMR spectrum in Figure 3B, significantly more complex product mixtures are produced. In addition to the expected polymer comprising dithiocarbonate R–O–C(=S)–S–R (OSS, δ(C<sup>q</sup> = S) = 212.2 ppm) links from formal alternating CS<sub>2</sub> and CHO insertion, one also observes monothiocarbonate R–O–C(=O)–S–R (OOS, δ(C<sup>q</sup> = O) = 169.1 ppm) and R–O–C(=S)–O–R (OSO, δ(C<sup>q</sup> = S) = 193.2 ppm) links as well as trithiocarbonate R–S–C(=S)–S–R (SSS, δ(C<sup>q</sup> = S) = 220.6 ppm) and carbonate R–O–C(=O)–O–R (OOO, δ(C<sup>q</sup> = S) = 153.9 ppm) links, which we could further evidence by Fourier transform infrared (FTIR) spectroscopy of the isolated polymer (Figure 3). Apart from polymeric (thio)carbonates, one also observes the formation of cyclohexene sulfide (CHS) and “unscrambled” cyclic five-membered dithiocarbonate (dt-c5c) as the only cyclic carbonate byproduct (Figure 3).

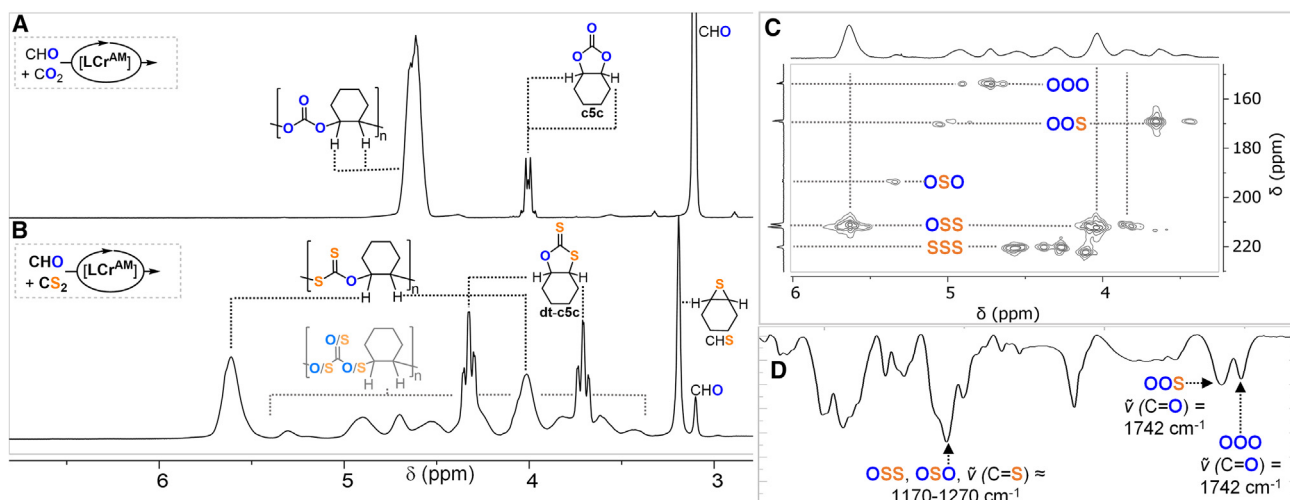


**Figure 3. Investigated copolymerizations**

(A)  $^1\text{H}$  NMR spectrum ( $\text{CDCl}_3$ , 400 MHz,  $25^\circ\text{C}$ ) of product mixture obtained from  $\text{CO}_2/\text{CHO}$  ROCOP corresponding to Table 1, run #6. (B)  $^1\text{H}$  NMR spectrum ( $\text{CDCl}_3$ , 400 MHz,  $25^\circ\text{C}$ ) of product mixture obtained from  $\text{CS}_2/\text{CHO}$  ROCOP corresponding to Table 1, run #11. (C and D)  $^1\text{H}$ - $^{13}\text{C}$  heteronuclear multiple bond correlation (HMBC) NMR ( $\text{CDCl}_3$ ,  $25^\circ\text{C}$ ) (C) and NMR FTIR (D) spectrum of precipitated polymer ROCOP corresponding to Table 1, run #11.

As for  $\text{CO}_2/\text{CHO}$  ROCOP, we observe an improvement in overall catalyst performance when moving to heavier AMs. While  $\text{LCr}^{\text{Li}}$  shows a low TOF of  $<5\text{ h}^{-1}$  and polymer selectivity of 12%,  $\text{LCr}^{\text{Na}}$  exhibits an overall improved performance (TOF =  $11 \pm 2\text{ h}^{-1}$ , 61% polymer selectivity). The heavier AMs in  $\text{LCr}^{\text{K/Rb/Cs}}$  all show a good polymer selectivity of 76% with improving linkage selectivity for the unscrambled OSS link when moving from K (37%) to Rb (53%) to Cs (58%). With regard to the catalyst rates, the maximum activities for  $\text{LCr}^{\text{K/Rb/Cs}}$  (TOF = 67–144  $\text{h}^{-1}$ ) all exceed those of  $\text{LCr}^{\text{Li}}$  and  $\text{LCr}^{\text{Na}}$ . For  $\text{LCr}^{\text{K}}$  and  $\text{LCr}^{\text{Cs}}$ , we observe an initiation period during which solubilization of the catalyst occurs. Nevertheless, one can clearly say that, as for  $\text{CO}_2/\text{CHO}$  ROCOP, the heavier AMs K, Rb, and Cs show improved performances in terms of both activity and selectivity over their lighter analogs, Li and Na, in the series of complexes  $\text{LCr}^{\text{AM}}$ . Hence, the order in catalyst performances exhibits clear parallels across ROCOPs. The copolymerizations yield materials with molecular weights ( $M_n = 5.4\text{--}15.6\text{ kDa}$ ) increasing with monomer conversions and somewhat broader molecular weight distributions ( $\mathcal{D} = 1.3\text{--}1.7$ ) than for  $\text{CO}_2/\text{CHO}$  ROCOP (Figure S15). Intrigued by the similarities in catalyst performance across ROCOPs, we turned to density functional theory (DFT) calculations (Notes S9 and S10) to characterize the mechanism of ROCOP at the  $\omega\text{B97XD, THF/BS2//}\omega\text{B97XD, THF/BS1}$  level of theory.  $\text{LCr}^{\text{Rb}}$  was chosen, and a monomeric form (in contrast to the dimers observed by XRD) was surveyed computationally in reference to prior studies.<sup>45</sup> Ethylene oxide was modeled as the epoxide substrate in place of the larger CHO utilized experimentally. Moreover, only one anionic coligand performing the catalysis, with the second kept as acetate serving as a spectator coligand, was modeled, where it speculated that the second carboxylate equivalent dissociates to create a vacant coordination site at the Cr center, as has been hypothesized in previous computational studies of heterobimetallic catalytic ROCOP.<sup>48</sup> A simplified mechanism in which one alternating monomer enchainment occurs was considered, as these steps must occur prior to other side reactions and allow for some general conclusions to be drawn regarding changes to the ROCOP mechanism and thus the kinetics when alternating the feedstock heteroallene. Starting from the model ethoxy intermediate A (stemming from epoxide ring opening), heteroallene

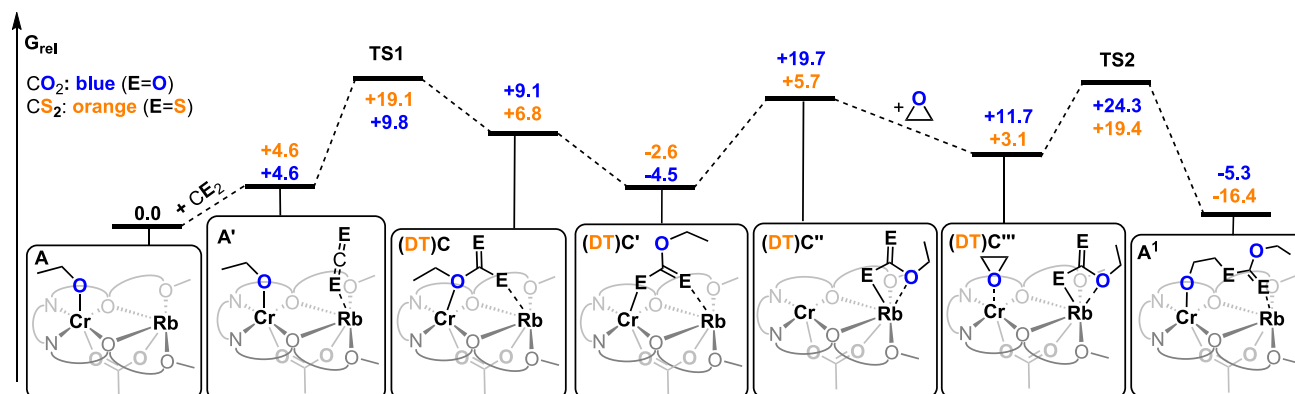


**Figure 4. Density functional theory of copolymerizations**

Computed free energy profile of simplified  $\text{CO}_2$ /epoxide and  $\text{CS}_2$ /epoxide ROCOP ( $\omega\text{B97XD, THF/BS2} // \omega\text{B97XD, THF/BS1}$  level of theory). Free energies reported are relative to **A** and given reactants and are quoted in kcal/mol. We note that a concerted (dithio)carbonate migration and epoxide addition process is plausible. While we have not modeled this step explicitly, we anticipate that such a barrier for this process is likely to lie lower in energy than that of  $(\text{DT})\text{C}'$ , and so this intermediate can be considered an upper limit to the barrier of this process, which still lies lower than **TS2**.

insertion to form the carbonate **C** or dithiocarbonate **DTC**, which then undergoes epoxide insertion to regenerate an extended alkoxide **A<sup>1</sup>**, was computationally characterized, the results of which are presented in Figure 4. As can be seen in Figure 4,  $\text{CE}_2$  activation occurs in both cases at **Rb** with the alkoxide ligand oriented at **Cr**. Heteroallene insertion via **TS1** is more kinetically facile for  $\text{CO}_2$  (+9.8 kcal mol<sup>-1</sup>) than for  $\text{CS}_2$  (+19.1 kcal mol<sup>-1</sup>), reflecting the decreased electrophilicity of the heavier homolog.<sup>49</sup> This forms dithiocarbonate complex **DTC** (+6.8 kcal mol<sup>-1</sup>) or carbonate complex **C** (+9.1 kcal mol<sup>-1</sup>), with subsequent (dithio)carbonate rearrangement to the **Cr** center taking place to afford the more thermodynamically favored species  $(\text{DT})\text{C}'$  at (-2.6) -4.5 kcal mol<sup>-1</sup>. Subsequent rearrangement of the (dithio)carbonate, whereby a switching of coordination to **Rb** in  $(\text{DT})\text{C}''$  (+5.7 kcal mol<sup>-1</sup>) and  $\text{C}''$  (+19.7 kcal mol<sup>-1</sup>) concomitantly reveals a vacant site at the **Cr** center to allow for subsequent epoxide coordination, forms  $(\text{DT})\text{C}'''$  (+3.1 kcal mol<sup>-1</sup>) and  $\text{C}'''$  (+11.7 kcal mol<sup>-1</sup>). This computed mechanism is consistent with reported computational studies of similar heterobimetallic catalytic ROCOP systems.<sup>48</sup> Ring opening via **TS2** then transforms the heterocarbonate coligand into an alkoxide **A<sup>1</sup>**, which, in both the cases of  $\text{CS}_2$  and  $\text{CO}_2$  ROCOP, is an overall exergonic process (where for  $\text{CO}_2$ ,  $\Delta G = -5.3$  kcal mol<sup>-1</sup>, and for  $\text{CS}_2$ ,  $\Delta G = -16.4$  kcal mol<sup>-1</sup>). From **A<sup>1</sup>**, addition of a second equivalent of heteroallene to form **A<sup>1'</sup>** thus initiates a second catalytic turnover and, relative to **A<sup>1</sup>**, is computed to be endergonic (where  $\text{A}^{1'S} = -12.2$  kcal mol<sup>-1</sup> and  $\text{A}^{1'O} = +3.6$  kcal mol<sup>-1</sup>) (see Note S10). Based on the energetic spans between **TS2** and  $(\text{DT})\text{C}'$  for the  $\text{CO}_2$  (+22.0 kcal mol<sup>-1</sup>) and  $\text{CS}_2$  (+28.8 kcal mol<sup>-1</sup>), epoxide ring opening is characterized as the rate-determining step in the case of both heteroallenes and is more kinetically facile for  $\text{CS}_2$ , which reflects the increase in nucleophilicity when moving down the periodic table and is well aligned with the lower reaction temperature that is required for  $\text{CS}_2$  than for  $\text{CO}_2$  ROCOP. Taken together, the computational study reveals that all favorable intermediates and transition states for the main propagation events are similar in structure for the two different heteroallenes, where alkoxide coordination at **Cr** and heteroallene activation at **Rb** as well as heterocarbonate coordination at **Rb** and epoxide activation at **Cr** prior to ring opening feature closely related geometries. The distinct roles of the cooperative partners are hence preserved from **O** to **S**, which we propose is the reason behind the maintenance of the activity order for  $\text{LCr}^{\text{AM}}$ . As epoxide ring opening is the rate-determining step for  $\text{E} = \text{O}$  and **S** in which

the nucleophilic heterocarbonate is oriented by the AM, we infer that the decrease in Lewis acidity when moving to heavier AMs leads to looser chain ends, which facilitates this insertion event and tentatively explains the increase in activity when moving from Li to Cs. Furthermore, moving to heavier AMs also introduces a more expanded coordination sphere, leading to a worse size match of those to the half-crown pocket of LCr. This could lead to decoordination of the AM during ROCOP as well as the potential for more complex aggregation in solution, both of which could lead to alternative propagation pathways to the one displayed in Figure 4. An interplay of those effects could, for example, explain why LCr<sup>Rb</sup> displays worse performance than LCr<sup>K</sup> even though Rb is the heavier AM.

### The O/S scrambling mechanism

In terms of side reactions, a loss of linkage (exemplified for LCr<sup>Rb</sup> from 53% to 16%) and polymer selectivity (from 76% to 35%) is observed when increasing the reaction temperature from 60°C to 100°C (Table 1, runs #10 and #12). Looking at the combined results presented in Table 1, it becomes clear that polymer and OSS linkage selectivity correlate, suggesting that dt-c5c generation and O/S scrambling occur through mechanistically related processes. In CO<sub>2</sub>/CHO ROCOP, it is well established that c5c formation occurs via backbiting of an alkoxide chain end into the adjacent carbonate link. Therefore, we presume that O/S scrambling occurs from side reactions of loosely coordinated alkoxide chain ends, and related hypotheses have been formulated previously that remain to be confirmed experimentally and computationally.<sup>35,36,38,40</sup> Bearing this hypothesis in mind, we turned toward elucidating the CS<sub>2</sub>/CHO ROCOP side-reaction mechanism. To experimentally survey the intermediates and side reactions (Note S5), we synthesized a model alkoxide A<sup>M</sup> choosing simple rubidium cyclohexyloxide RbOCy to avoid the paramagnetism of Cr. Addition of 5 equiv CS<sub>2</sub> at ambient temperature in THF (Figure 5A) leads to quantitative formation of the related rubidium dithiocarbonate RbSC(=S)OCy DTC<sup>M</sup> ( $\delta(\text{C}^{\text{q}} = \text{S}) = 229.9$  ppm). Attempting to regenerate an alkoxide, we added 1 equiv CHO to DTC<sup>M</sup> in d<sup>6</sup>-DMSO at ambient temperature but did not observe any CHO ring opening, further supporting epoxide insertion as the rate-determining step of CS<sub>2</sub>/CHO ROCOP. Heating the reaction mixture at 100°C for 30 min results in CHO ring opening forming a complex reaction mixture instead of the expected dithiocarbonate-appended alkoxide A<sup>M1</sup> (Figure 5A). NMR and IR analyses reveal the formation of the rubidium monothiocarbonate RbSC(=O)OCy MTC<sup>M</sup> ( $\delta(\text{C}^{\text{q}} = \text{O}) = 183.0$  ppm, and  $\tilde{\nu}(\text{C}=\text{O}) = 1,587$  cm<sup>-1</sup>) as well as poly(CHS) alongside the precipitation of the rubidium carbonate RbOC(=O)OCy C<sup>M</sup> ( $\tilde{\nu}(\text{C}=\text{O}) = 1,657$  cm<sup>-1</sup>). Isolated MTC<sup>M</sup> (*vide infra*) likewise only reacts with CHO upon heating to 100°C in d<sub>6</sub>-DMSO with precipitation of C<sup>M</sup> and poly(CHS) formation. This indicates that the generation of heterocarbonates other than DTC and OSS occurs rapidly following CHO insertion, which leads to oxygen-enriched carbonates and deployment of the excess sulfur in thiirane byproducts. We believe the nucleophilic attack of the metal alkoxide into the adjacent dithiocarbonate link in A<sup>M1</sup> to be the entry point to this process. To confirm this hypothesis, we reacted A<sup>M</sup> with the dithiocarbonate dt-c5c and the monothiocarbonate mt-c5c in THF at ambient temperature (Figure 5B). Reacting A<sup>M</sup> with dt-c5c results in instant discoloration and precipitation of a colorless solid, which we could identify as MTC<sup>M</sup>. Additionally, <sup>1</sup>H NMR analysis of the supernatant solution unambiguously reveals the formation of CHS. Likewise, reacting A<sup>M</sup> with mt-c5c leads to precipitation of C<sup>M</sup> and thiirane generation. In reference to previous hypotheses by Werner and co-workers, we propose a reaction pathway (Figure 6B) in which the metal alkoxide attack into organic (di)thiocarbonates generates a tetrahedral intermediate I, which collapses into an oxygen-enriched organic (thio)carbonate-appended metal thiolate T that can eliminate thiirane to release MTC<sup>M</sup> or

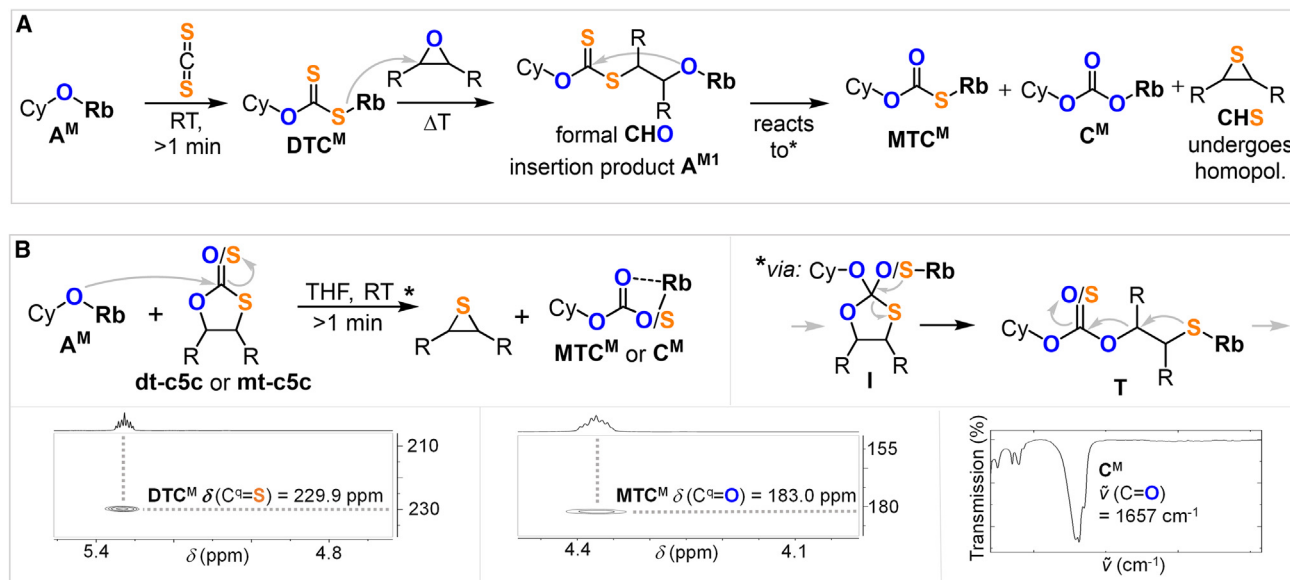


**Figure 5. Model reactions for the scrambling mechanism**

(A) Generation of  $\text{DTC}^{\text{M}}$  from  $\text{A}^{\text{M}}$  and observed reaction between  $\text{DTC}^{\text{M}}$  and CHO.

(B) Reaction of  $\text{A}^{\text{M}}$  with the cyclic (di)thiocarbonates **dt-c5c** and **mt-c5c** as well as  $^1\text{H}$   $^{13}\text{C}$  HMBC spectra of  $\text{DTC}^{\text{M}}$  and  $\text{MTC}^{\text{M}}$  and FTIR spectrum of  $\text{C}^{\text{M}}$ . Cy,  $\text{C}_6\text{H}_{11}$ ; R,  $-\text{C}_4\text{H}_8-$ , H.

$\text{C}^{\text{M}}$ .<sup>35</sup> This substantiates the hypothesis that O/S scrambling occurs via alkoxide originated backbiting pathways and also explains the thiirane byproducts observed during  $\text{CS}_2/\text{CHO}$  ROCOP. Knowing the origin of O/S scrambling, one can formulate a  $\text{CS}_2/\text{CHO}$  propagation mechanism explaining the product distribution. Initially in the primary propagation cycle (Figure 6A), alternating  $\text{CS}_2$  insertion starting from the alkoxide intermediate **A** gives **DTC**, which then inserts CHO, generating OSS links sitting adjacent to metal alkoxide chain-end  $\text{A}^1$ . Backbiting generates a tetrahedral intermediate **I** that, in one instance, can eliminate **dt-c5c** to regenerate **A**. Alternatively, **I** can rearrange into a metal thiolate chain-end **T**, generating an OSO link and resulting in O/S scrambling between the chain end and the adjacent heterocarbonate link. From **T** thiirane elimination generates a metal monothiocarbonate chain-end **MTC** that then continues to propagate. In order to assess the energetic feasibility of these reaction pathways, we again turned to DFT. As displayed in Figure 6B, initial backbiting from  $\text{A}^1$  takes place via **TS3** (+21.7 kcal mol<sup>-1</sup>) to form **I** (+14.0 kcal mol<sup>-1</sup>). From **I**, release of **dt-c5c** takes place initially via rearrangement of the ligated heterocycle to form **I'** (+18.3 kcal mol<sup>-1</sup>) and subsequent C–O cleavage via **TS4** (+21.1 kcal mol<sup>-1</sup>) to form **I(dt-c5c)** (–1.2 kcal mol<sup>-1</sup>). Alternatively, from **I**, a series of rearrangements of the ligated heterocyclic group (via **TS5**, **I''**, and **TS6**) ultimately yields **I'''** (+3.7 kcal mol<sup>-1</sup>). Ring opening can then take place from this species via **TS7** (+18.7 kcal mol<sup>-1</sup>) to form **T** (+8 kcal mol<sup>-1</sup>) to finalize the O/S scrambling process, followed by rearrangement of the ring-opened chain to exergonically afford **T'** (–8.3 kcal mol<sup>-1</sup>). The calculations thus indicate that O/S exchange is kinetically accessible, where the largest energetic span of the process is 23.3 kcal mol<sup>-1</sup>, and exergonic overall ( $\Delta G$  from  $\text{A}^1 = -8.3$  kcal mol<sup>-1</sup>). This indicates that O/S scrambling is thermodynamically driven owing to the more favorable accumulation of negative charge on S compared with O, suggesting that future catalyst endeavors to suppress O/S scrambling should employ more oxophilic metals than Cr to disfavor thiolate formation. From **T'**, thiirane formation via C–O cleavage and concomitant transfer of the electrophilic C center to the Cr-bound thiolate group

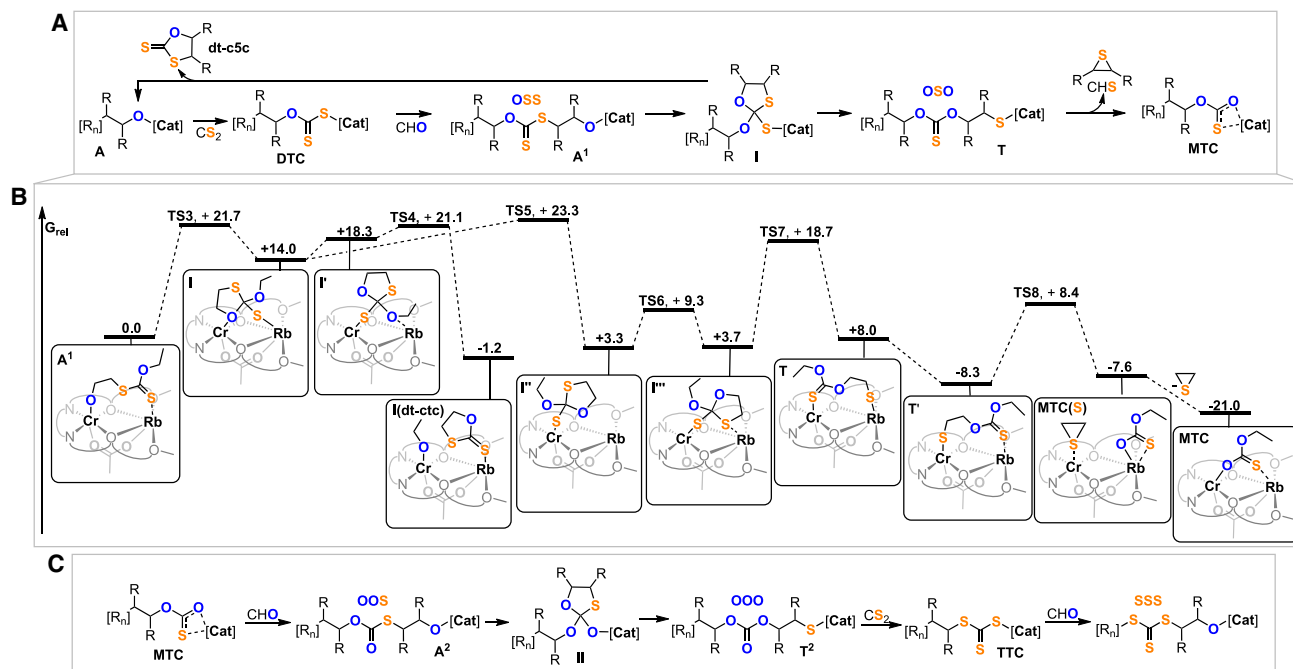


**Figure 6. Density functional theory of the scrambling mechanism**

(A and B) Part 1 of the mechanistic hypothesis of  $\text{CS}_2/\text{CHO}$  ROCOP explaining (A) the different linkage isomers and byproducts as well as the (B) computed free energy profile ( $\omega\text{B97XD, THF/BS2}/\omega\text{B97XD, THF/BS1}$  level of theory). (C) Part 2 of the mechanistic hypothesis.

via **TS8** (+8.4 kcal mol<sup>-1</sup>) is identified to be kinetically accessible, with an overall activation barrier of +16.7 kcal mol<sup>-1</sup> to form **MTC(S)** (−7.6 kcal mol<sup>-1</sup>). Onward, thiirane release is then characterized to form **MTC** (−21.0 kcal mol<sup>-1</sup>), which is structurally related to **DTC** and **C** (*vide supra*) and favors a bridged thiocarboxylate coligand. Therefore, the energetics of these side processes are in agreement with the experiment identifying them as kinetically and thermodynamically viable and in competition with copolymerization. Having computationally verified the viability of the key events in O/S scrambling, one can explain the formation of the other links with closely related reaction steps (Figure 6B). CHO insertion by **MTC** forms an OOS link-appended metal-alkoxide chain-end **A<sup>2</sup>**. A backbiting process like the prior one through **II** leads again to O/S scrambling between the chain end and the adjacent heterocarbonate link, generating a metal-thiolate chain-end **T<sup>2</sup>** and an all-oxygen **OOO** link. Generation of all-sulfur **SSS** links can be rationalized by  $\text{CS}_2$  insertion into metal thiolate chain ends forming metal trithiocarbonate chain-end **TTC** followed by propagation. As we have shown above (Figure 4) that formal O-to-S substitution has little effect on the intermediate- and transition-state geometries, we infer this is also the case for **MTC** and **TTC** and so metal-metal cooperativity is also maintained in these steps. Finally, it should be noted that the scrambling processes that have been formulated at the chain end can likewise occur by attack of alkoxide chain ends into any heterocarbonate link of the chain, which could at least partially explain the broadened ( $\text{Đ} > 1.3\text{--}1.7$ ) molecular weight distributions of the  $\text{CS}_2$  copolymers.<sup>50</sup>

### **CO<sub>2</sub>/CS<sub>2</sub>/epoxide ring-opening terpolymerization and degradation experiments**

Owing to the mechanistic similarities between the  $\text{CO}_2$  and the  $\text{CS}_2$  ROCOP process, we suspected their ring-opening terpolymerization (ROTERP) to be feasible

**Table 2. Data showing CO<sub>2</sub>/CS<sub>2</sub>/epoxide ROTERP under different conditions**

Run	CS <sub>2</sub> equiv <sup>a</sup>	t (h)	TON <sup>b</sup>	TOF (h <sup>-1</sup> ) <sup>c</sup>	Pol. (%) <sup>d</sup>	OOO (%) <sup>e</sup>	M <sub>n</sub> (kDa) (Đ) <sup>f</sup>
#1	500	5	634	127	95	95	11.6 (1.3)
#2	1,000	5	715	143	91	83	12.7 (1.6)
#3	2,000	5	500	100	82	77	9.4 (1.4)
#4	3,000	7	570	81	53	64	4.7 (1.5)

<sup>a</sup>Copolymerization at 1 equiv LM<sup>AM</sup>: 1,000 equiv CHO: varying equiv CS<sub>2</sub>, T = 100°C.

<sup>b</sup>Turnover number (TON), number of moles of CHO/CHS coupled to heterocarboxates per mole of catalyst.

<sup>c</sup>Turnover frequency (TOF) as TON/time.

<sup>d</sup>Relative integrals in the normalized <sup>1</sup>H NMR spectrum (CDCl<sub>3</sub>, 25°C, 400 MHz) of tertiary CH resonances due to polymeric relative to cyclic heterocarboxates.

<sup>e</sup>Relative integrals in the normalized <sup>1</sup>H NMR spectrum of tertiary CH resonances due to OOO vs. other heterocarboxate links.

<sup>f</sup>Determined by GPC (gel permeation chromatography) measurements conducted in THF, using narrow MW polystyrene standards to calibrate the instrument.

(Note S6). Accordingly we performed CO<sub>2</sub>/CS<sub>2</sub>/CHO ROTERP at 100°C employing LCr<sup>Rb</sup> (1 equiv LCr<sup>Rb</sup>: 1,000 equiv CHO: 500–3,000 equiv CS<sub>2</sub> under 4 bar CO<sub>2</sub> pressure), and the results are summarized in Table 2. Under these conditions, the terpolymerization can be performed in screw cap glass vessels with tightly attached tubing as the applied overpressure increases the boiling point of the reaction mixture sufficiently, which obviates the need for steel reactor setups. In all cases, we observe successful terpolymer formation in good to excellent polymer yields of 53%–95% with respect to dt-c5c as the only cyclic carbonate byproduct. We observe preferential formation of OOO linkages (64%–95%) with increasing proportions of sulfurated links when more CS<sub>2</sub> is employed in the starting mixture. This suggests preferential carbon dioxide incorporation during ROCOP due to kinetically favored CO<sub>2</sub> over CS<sub>2</sub> insertion by metal-alkoxide intermediate as predicted by our computational studies. NMR analysis of the terpolymers shows that all heterocarboxate links observed in CS<sub>2</sub>/CHO ROCOP, i.e., OOS, OSO, OSS, and SSS, are incorporated in the terpolymer, with OOS and SSS links being the most prominent (80%–90%) ones irrespective of the starting feed ratio (Figure 7). Moving to lower temperatures (80°C) or higher CO<sub>2</sub> pressure (20 bar) results in no sulfur incorporation on the <sup>1</sup>H NMR, while higher temperatures (120°C) only yield oligomeric products (M<sub>n</sub> < 2 kDa). Monitoring a ROTERP reaction by aliquot NMR analysis reveals that all links form in constant proportion throughout the ROTERP process, supporting random, as opposed to gradient, terpolymerization. The ROTERP methodology yields terpolymers with molecular weights M<sub>n</sub> = 4.7–12.6 kDa (Đ = 1.3–1.6), which formally constitute CO<sub>2</sub>-derived polycarbonates with a few randomly interspersed sulfur centers. Consequently, they are brittle materials with a T<sub>g</sub> of 85.3°C and a refractive index of 1.49 for run #2 in Table 2, which is very similar to the values for all oxygen variants with a T<sub>g</sub> of 90.4 and a refractive index of 1.48 for run #4 in Table 1. However, we were intrigued to see how polycarbonate sulfuration affects the degradability of the material given that sulfur-containing polymers are susceptible to oxidative and photolytic breakdown (Note S7).<sup>51,52</sup> Hence, we initially investigated oxidative disassembly of the respective CS<sub>2</sub> or CO<sub>2</sub>/CHO copolymer (Table 1, runs #4 and #11). Immersion in aqueous H<sub>2</sub>O<sub>2</sub> overnight leads to complete disintegration of the CS<sub>2</sub>/CHO copolymer, with no polymeric products detectable by gel permeation chromatography (GPC).

The initially highly hydrophobic and yellow polymer turns into colorless degradation products that homogeneously disperse in the aqueous medium, indicating increasing hydrophilicity and loss of the yellow C=S chromophores during degradation. <sup>1</sup>H

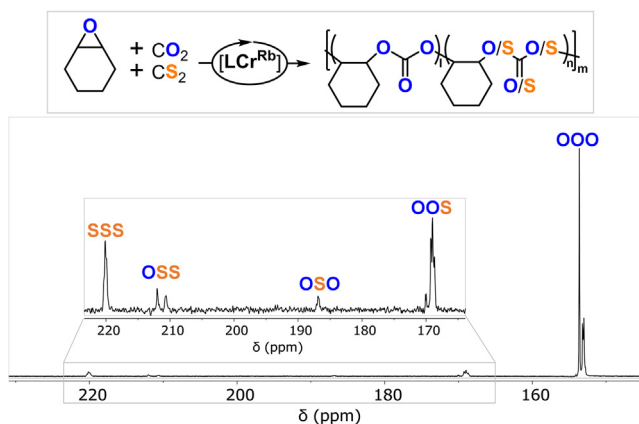


**Figure 7. Terpolymerization scheme**

Schematic summarizing  $\text{CO}_2/\text{CS}_2/\text{CHO}$  ROTERP methodology and zoom into the carbonyl region of an associated  $\text{C}^{13}\text{H}$  NMR spectrum ( $\text{CDCl}_3$ , 126 MHz, 25°C, Table 2, run #2).

NMR analysis of the degradation products shows the complete disappearance of resonance associated with  $\text{C}=\text{S}$ -containing links, while  $\text{C}=\text{O}$ -containing links remain intact. IR analysis of the decomposition products reveals emergence of bands at ca.  $\tilde{\nu} = 1,150$  and  $1,250 \text{ cm}^{-1}$ , which are indicative of  $\text{S}=\text{O}$  from, e.g., sulfone or sulfonic acid groups, and our results therefore indicate degradation via oxidation of the sulfur centers. Accordingly, the all-oxygen  $\text{CO}_2/\text{CHO}$  copolymer stays fully intact under the same conditions. Gratifyingly, the  $\text{CO}_2/\text{CS}_2/\text{CHO}$  terpolymers (Table 2, runs #1 and #2) degrade into oligomeric products with  $M_n \approx 2 \text{ kg/mol}$ . NMR analysis of the produced mixture reveals that the resonances associated with the  $\text{OOO}$  links of the terpolymer remain unaffected by the oxidation process, while the resonances associated with the sulfurated links partially disappear and shift (Figure 8B), confirming that the sulfur-containing links act as preinstalled oxidatively labile breaking points (Figure 8A). Next, we turned toward UV degradation of our materials (Table 1, runs #4 and #10). UV irradiation of the  $\text{CS}_2/\text{CHO}$  copolymer in  $\text{CDCl}_3$  solution for 24 h leads to complete disintegration of the material, with no polymeric products detectable by size-exclusion chromatography (SEC). NMR analysis of the degradation products shows emergence of alkene resonances ( $\delta (^1\text{H}) = 5.7 \text{ ppm}$ ;  $\delta (^{13}\text{C}) = 127.5 \text{ ppm}$ ), indicating degradation via Chugaev elimination pathways. Accordingly, FTIR analysis of the reaction headspace reveals the formation of  $\text{CS}_2$  and  $\text{COS}$ . In contrast, the all-oxygen analog  $\text{CO}_2/\text{CHO}$  polycarbonate stays fully intact under the same conditions. However, the  $\text{CO}_2/\text{CS}_2/\text{CHO}$  terpolymers (Table 2, runs #1 and #2) degrade into oligomeric products with  $M_n \approx 2 \text{ kg/mol}$  upon UV irradiation (Figure 8C). Our results hence show that the sulfur-containing links also act as predetermined photochemical breaking points in the otherwise robust polycarbonates. Sulfuration of as few as ca. 1 out of 20 links (Table 2, run #1) lets the material access complementary degradation pathways.

In conclusion we have presented a comprehensive study on  $\text{CO}_2/\text{CHO}$  and  $\text{CS}_2/\text{CHO}$  ROCOP employing a series of new heterobimetallic catalysts, which eventually allowed us to combine both processes in  $\text{CO}_2/\text{CS}_2/\text{CHO}$  ROTERP. We found that heterobimetallic cooperativity in terms of rate and selectivity is maintained when moving from  $\text{CO}_2$  to  $\text{CS}_2$ , which is due to structurally analogous rate-determining steps that are more easily overcome with less Lewis-acidic AMs. We found the mechanistic origin behind O/S scrambling to be backbiting reactions in which metal alkoxide chain ends attack heterocarbonate links. Hereby, those

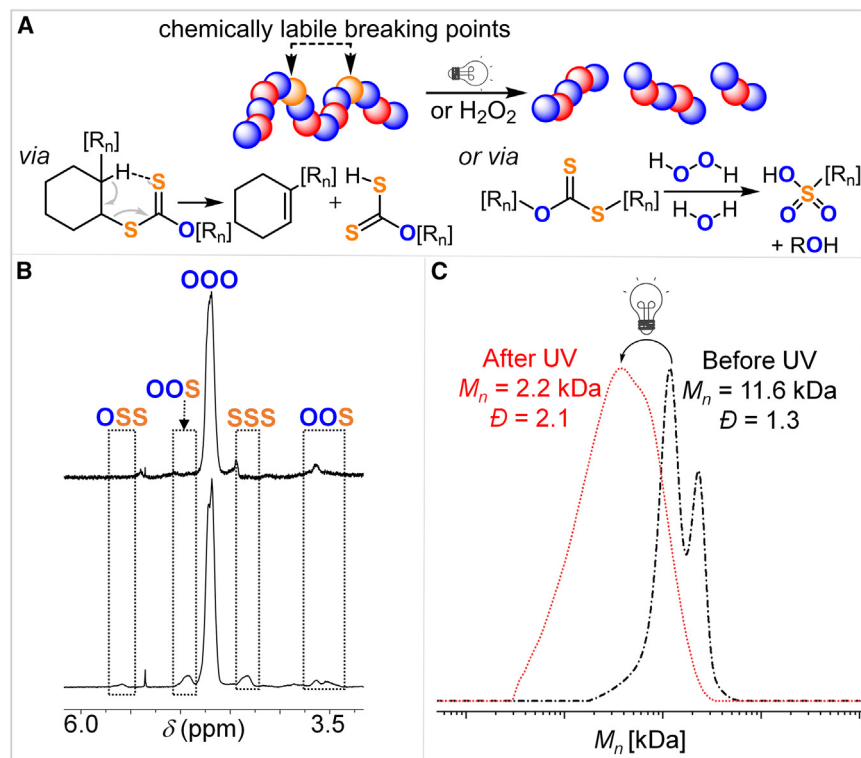


**Figure 8. Degradation experiments**

(A) Sulfurated links act as breaking points; red balls denote  $CO_2$  monomers.

(B)  $^1H$  NMR spectra ( $CDCl_3$ , 400 MHz, 25°C) of terpolymer (corresponding to Table 2, run #2) before and after treatment with  $H_2O_2$ .

(C) SEC traces before and after photolytic breakdown (corresponding to Table 2, run #1).

transform into metal thiolate chain ends under oxygen enrichment of the adjacent (hetero)carbonate links, which then themselves either eliminate thiiranes to form metal(hetero)carbonate chain ends or propagate. The fact that  $CS_2/CHO$  ROCOP can be understood as a series of interconnected ROCOP cycles eventually allowed for  $CO_2/CS_2/CHO$  ROTERP to generate polycarbonates with some interspersed sulfur-containing linkages. Sulfuration of as few as one out of 20 heterocarbonate links was found to impart chemical and photodegradability onto the parent  $CO_2$  copolymers, which is attractive given that oxidation and photolysis represent the initial breakdown pathways of polymer waste in nature. Our study demonstrates how mechanistic understanding can allow the control of complex catalytic systems for the valorization of  $CO_2$  into new degradable materials, which could be transferable to many other ring-opening polymerizations.

## EXPERIMENTAL PROCEDURES

### Resource availability

#### Lead contact

Further information and requests for resources should be directed to and will be fulfilled by the lead contact, Alex J. Plajer ([plajer@zedat.fu-berlin.de](mailto:plajer@zedat.fu-berlin.de)).

#### Materials availability

All materials generated in this study are available from the lead contact without restriction.

### Data and code availability

The authors declare that the data supporting the findings of this study are available within the article and the [supplemental information](#).

Single-crystal X-ray data are available at the Cambridge Crystallographic Database under the identification codes CCDC: 2243753, 2243925, 2243420, 2242774, 2243903, and 2243785.

All other data are available from the [lead contact](#) upon reasonable request.

### Methods

See the [supplemental information](#) for full details of synthesis, characterization, and analysis in [Notes S1–S10](#).

### SUPPLEMENTAL INFORMATION

Supplemental information can be found online at <https://doi.org/10.1016/j.xcrp.2023.101510>.

### ACKNOWLEDGMENTS

The VCI is acknowledged for a Liebig Fellowship to A.J.P. Christian Müller and Prof. Dr. Rainer Haag are thanked for continuous support and valuable discussions. Thomas Rybak and Prof. Dr. Bernhard Scharfel (Bundesanstalt für Materialforschung Fachbereich 7.5) are thanked for DSC measurements.

### AUTHOR CONTRIBUTIONS

J.S., M.R.S., and A.J.P. performed the experiments and analyzed the data. S.M.R. collected and analyzed the XRD data. S.N. performed the DFT calculations. A.J.P. and S.N. wrote the manuscript and supplemental information. A.J.P. secured the funding and designed and directed the project.

### DECLARATION OF INTERESTS

The authors declare no competing interests.

Received: April 3, 2023

Revised: May 23, 2023

Accepted: June 23, 2023

Published: July 21, 2023

### REFERENCES

1. Crockett, M.P., Evans, A.M., Worthington, M.J.H., Albuquerque, I.S., Slattery, A.D., Gibson, C.T., Campbell, J.A., Lewis, D.A., Bernardes, G.J.L., and Chalker, J.M. (2016). Sulfur-Limonene Polysulfide: A Material Synthesized Entirely from Industrial By-Products and Its Use in Removing Toxic Metals from Water and Soil. *Angew. Chem. Int. Ed.* 55, 1714–1718.
2. Braatz, D., Cherri, M., Tully, M., Dimde, M., Ma, G., Mohammadifar, E., Reisbeck, F., Ahmadi, V., Schirner, M., and Haag, R. (2022). Chemical Approaches to Synthetic Drug Delivery Systems for Systemic Applications. *Angew. Chem. Int. Ed.* 61.
3. Wang, Y., Li, M., Chen, J., Tao, Y., and Wang, X. (2021). O-to-S Substitution Enables Dovetailing Conflicting Cyclizability, Polymerizability, and Recyclability: Dithiolactone vs. Dilactone. *Angew. Chem. Int. Ed. Engl.* 60, 22547–22553.
4. Shi, C., McGraw, M.L., Li, Z.-C., Cavallo, L., Falivene, L., and Chen, E.Y.-X. (2020). High-performance pan-tactic polythioesters with intrinsic crystallinity and chemical recyclability. *Sci. Adv.* 6, eabc0495.
5. Li, H., Ollivier, J., Guillaume, S.M., and Carpentier, J.-F. (2022). Tacticity Control of Cyclic Poly(3-Thiobutyrates) Prepared by Ring-Opening Polymerization of Racemic  $\beta$ -Thiobutyrolactone. *Angew. Chem. Int. Ed.* 61, e202202386.
6. Haider, T.P., Völker, C., Kramm, J., Landfester, K., and Wurm, F.R. (2019). Plastics of the Future? The Impact of Biodegradable Polymers on the Environment and on Society. *Angew. Chem. Int. Ed.* 58, 50–62.
7. Yuan, P., Sun, Y., Xu, X., Luo, Y., and Hong, M. (2022). Towards high-performance sustainable polymers via isomerization-driven irreversible ring-opening polymerization of five-membered thionolactones. *Nat. Chem.* 14, 294–303.
8. Baur, M., Lin, F., Morgen, T.O., Odenwald, L., and Mecking, S. (2021). Polyethylene materials with in-chain ketones from nonalternating catalytic copolymerization. *Science* 374, 604–607.
9. Plajer, A.J., and Williams, C.K. (2022). Heterocycle/Heteroallene Ring-Opening

- Copolymerization: Selective Catalysis Delivering Alternating Copolymers. *Angew. Chem. Int. Ed.* **61**, e202104495.
10. Longo, J.M., Sanford, M.J., and Coates, G.W. (2016). Ring-Opening Copolymerization of Epoxides and Cyclic Anhydrides with Discrete Metal Complexes: Structure–Property Relationships. *Chem. Rev.* **116**, 15167–15197.
  11. Lu, X.-B., Ren, W.-M., and Wu, G.-P. (2012). CO<sub>2</sub> Copolymers from Epoxides: Catalyst Activity, Product Selectivity, and Stereochemistry Control. *Acc. Chem. Res.* **45**, 1721–1735.
  12. Yang, G.-W., Zhang, Y.-Y., and Wu, G.-P. (2021). Modular Organoboron Catalysts Enable Transformations with Unprecedented Reactivity. *Acc. Chem. Res.* **54**, 4434–4448.
  13. Jia, M., Hadjichristidis, N., Gnanou, Y., and Feng, X. (2021). Polyurethanes from Direct Organocatalytic Copolymerization of *p*-Tosyl Isocyanate with Epoxides. *Angew. Chem. Int. Ed.* **60**, 1593–1598.
  14. Xu, J., and Hadjichristidis, N. (2021). Well-Defined Poly(Ester Amide)-Based Homo- and Block Copolymers by One-Pot Organocatalytic Anionic Ring-Opening Copolymerization of *N*-Sulfonyl Aziridines and Cyclic Anhydrides. *Angew. Chem. Int. Ed.* **60**, 6949–6954.
  15. Xu, J., Wang, X., and Hadjichristidis, N. (2021). Diblock dialternating terpolymers by one-step/one-pot highly selective organocatalytic multimonomer polymerization. *Nat. Commun.* **12**, 7124.
  16. Lidston, C.A.L., Severson, S.M., Abel, B.A., and Coates, G.W. (2022). Multifunctional Catalysts for Ring-Opening Copolymerizations. *ACS Catal.* **12**, 11037–11070.
  17. Kernbichl, S., Reiter, M., Adams, F., Vagin, S., and Rieger, B. (2017). CO<sub>2</sub>-Controlled One-Pot Synthesis of AB, ABA Block, and Statistical Terpolymers from  $\beta$ -Butyrolactone, Epoxides, and CO<sub>2</sub>. *J. Am. Chem. Soc.* **139**, 6787–6790.
  18. Lee, T., Dirlam, P.T., Njardarson, J.T., Glass, R.S., and Pyun, J. (2022). Polymerizations with Elemental Sulfur: From Petroleum Refining to Polymeric Materials. *J. Am. Chem. Soc.* **144**, 5–22.
  19. Yang, J.-L., Wu, H.-L., Li, Y., Zhang, X.-H., and Darensbourg, D.J. (2017). Perfectly Alternating and Regioselective Copolymerization of Carbonyl Sulfide and Epoxides by Metal-Free Lewis Pairs. *Angew. Chem. Int. Ed.* **56**, 5774–5779.
  20. Yue, T.-J., Ren, W.-M., Chen, L., Gu, G.-G., Liu, Y., and Lu, X.-B. (2018). Synthesis of Chiral Sulfur-Containing Polymers: Asymmetric Copolymerization of meso-Epoxides and Carbonyl Sulfide. *Angew. Chem. Int. Ed.* **57**, 12670–12674.
  21. Zhu, X.-F., Yang, G.-W., Xie, R., and Wu, G.-P. (2022). One-Pot Construction of Sulfur-Rich Thermoplastic Elastomers Enabled by Metal-Free Self-Switchable Catalysis and Air-Assisted Coupling. *Angew. Chem. Int. Ed.* **61**, e202115189.
  22. Chao, J., Yue, T., Ren, B., Gu, G., Lu, X., and Ren, W. (2022). Controlled Disassembly of Elemental Sulfur: An Approach to the Precise Synthesis of Polydisulfides. *Angew. Chem. Int. Ed.* **61**, e202115950.
  23. Yue, T.-J., Zhang, M.-C., Gu, G.-G., Wang, L.-Y., Ren, W.-M., and Lu, X.-B. (2019). Precise Synthesis of Poly(thioester)s with Diverse Structures by Copolymerization of Cyclic Thioanhydrides and Episulfides Mediated by Organic Ammonium Salts. *Angew. Chem. Int. Ed.* **58**, 618–623.
  24. Rupf, S., Pröhm, P., and Plajer, A.J. (2022). Lithium achieves sequence selective ring-opening terpolymerisation (ROTERP) of ternary monomer mixtures. *Chem. Sci.* **13**, 6355–6365.
  25. Nakano, K., Tatsumi, G., and Nozaki, K. (2007). Synthesis of Sulfur-Rich Polymers: Copolymerization of Episulfide with Carbon Disulfide by Using [PPN]Cl/(salph)Cr(III)Cl System. *J. Am. Chem. Soc.* **129**, 15116–15117.
  26. Chung, W.J., Griebel, J.J., Kim, E.T., Yoon, H., Simmonds, A.G., Ji, H.J., Dirlam, P.T., Glass, R.S., Wie, J.J., Nguyen, N.A., et al. (2013). The use of elemental sulfur as an alternative feedstock for polymeric materials. *Nat. Chem.* **5**, 518–524.
  27. Kang, K.-S., Olikagu, C., Lee, T., Bao, J., Molineux, J., Holmen, L.N., Martin, K.P., Kim, K.-J., Kim, K.H., Bang, J., et al. (2022). Sulfenyl Chlorides: An Alternative Monomer Feedstock from Elemental Sulfur for Polymer Synthesis. *J. Am. Chem. Soc.* **144**, 23044–23052.
  28. Jia, J., Liu, J., Wang, Z.-Q., Liu, T., Yan, P., Gong, X.-Q., Zhao, C., Chen, L., Miao, C., Zhao, W., et al. (2022). Photoinduced inverse vulcanization. *Nat. Chem.* **14**, 1249–1257.
  29. Wang, L.-Y., Gu, G.-G., Ren, B.-H., Yue, T.-J., Lu, X.-B., and Ren, W.-M. (2020). Intramolecularly Cooperative Catalysis for Copolymerization of Cyclic Thioanhydrides and Epoxides: A Dual Activation Strategy to Well-Defined Polythioesters. *ACS Catal.* **10**, 6635–6644.
  30. Yue, T.-J., Bhat, G.A., Zhang, W.-J., Ren, W.-M., Lu, X.-B., and Darensbourg, D.J. (2020). Facile Synthesis of Well-Defined Branched Sulfur-Containing Copolymers: One-Pot Copolymerization of Carbonyl Sulfide and Epoxide. *Angew. Chem. Int. Ed.* **59**, 13633–13637.
  31. Yue, T.-J., Ren, B.-H., Zhang, W.-J., Lu, X.-B., Ren, W.-M., and Darensbourg, D.J. (2021). Randomly Distributed Sulfur Atoms in the Main Chains of CO<sub>2</sub>-Based Polycarbonates: Enhanced Optical Properties. *Angew. Chem. Int. Ed.* **60**, 4315–4321.
  32. Silbernagl, D., Sturm, H., and Plajer, A.J. (2022). Thioanhydride/isothiocyanate/epoxide ring-opening terpolymerisation: sequence selective enchainment of monomer mixtures and switchable catalysis. *Polym. Chem.* **13**, 3981–3985.
  33. Plajer, A.J. (2022). Sequence selective ring-opening terpolymerisation facilitates higher order switchable catalysis. *ChemCatChem* **14**, e202200867. <https://doi.org/10.1002/cctc.202200867>.
  34. McGuire, T.M., and Buchard, A. (2021). Polymers from sugars and CS<sub>2</sub>: ring opening copolymerisation of a D-xylose anhydrosugar oxetane. *Polym. Chem.* **12**, 4253–4261.
  35. Diebler, J., Komber, H., Häußler, L., Lederer, A., and Werner, T. (2016). Alkoxide-Initiated Regioselective Coupling of Carbon Disulfide and Terminal Epoxides for the Synthesis of Strongly Alternating Copolymers. *Macromolecules* **49**, 4723–4731.
  36. Darensbourg, D.J., Wilson, S.J., and Yeung, A.D. (2013). Oxygen/Sulfur Scrambling During the Copolymerization of Cyclopentene Oxide and Carbon Disulfide: Selectivity for Copolymer vs Cyclic [Thio]carbonates. *Macromolecules* **46**, 8102–8110.
  37. Yang, Z., Hu, C., Cui, F., Pang, X., Huang, Y., Zhou, Y., and Chen, X. (2022). One-Pot Precision Synthesis of AB, ABA and ABC Block Copolymers via Switchable Catalysis. *Angew. Chem. Int. Ed.* **61**, e202117533.
  38. Luo, M., Zhang, X.-H., and Darensbourg, D.J. (2015). An Investigation of the Pathways for Oxygen/Sulfur Scramblings during the Copolymerization of Carbon Disulfide and Oxetane. *Macromolecules* **48**, 5526–5532.
  39. Zhang, X.-H., Liu, F., Sun, X.-K., Chen, S., Du, B.-Y., Qi, G.-R., and Wan, K.M. (2008). Atom-Exchange Coordination Polymerization of Carbon Disulfide and Propylene Oxide by a Highly Effective Double-Metal Cyanide Complex. *Macromolecules* **41**, 1587–1590.
  40. Darensbourg, D.J., Andreatta, J.R., Jungman, M.J., and Reibenspies, J.H. (2009). Investigations into the coupling of cyclohexene oxide and carbon disulfide catalyzed by (salen)CrCl. Selectivity for the production of copolymers vs. cyclic thiocarbonates. *Dalton Trans.* 8891–8899.
  41. Diment, W.T., Lindeboom, W., Fiorentini, F., Deacy, A.C., and Williams, C.K. (2022). Synergic Heterodinuclear Catalysts for the Ring-Opening Copolymerization (ROCOP) of Epoxides, Carbon Dioxide, and Anhydrides. *Acc. Chem. Res.* **55**, 1997–2010.
  42. Gruszka, W., and Garden, J.A. (2021). Advances in heterometallic ring-opening (co) polymerisation catalysis. *Nat. Commun.* **12**, 3252.
  43. Thevenon, A., Garden, J.A., White, A.J.P., and Williams, C.K. (2015). Dinuclear Zinc Salen Catalysts for the Ring Opening Copolymerization of Epoxides and Carbon Dioxide or Anhydrides. *Inorg. Chem.* **54**, 11906–11915.
  44. Deacy, A.C., Durr, C.B., Kerr, R.W.F., and Williams, C.K. (2021). Heterodinuclear catalysts Zn(II)/M and Mg(II)/M, where M = Na(I), Ca(II) or Cd(II), for phthalic anhydride/cyclohexene oxide ring opening copolymerisation. *Catal. Sci. Technol.* **11**, 3109–3118.
  45. Diment, W.T., Gregory, G.L., Kerr, R.W.F., Phanopoulos, A., Buchard, A., and Williams, C.K. (2021). Catalytic Synergy Using Al(III) and Group 1 Metals to Accelerate Epoxide and Anhydride Ring-Opening Copolymerizations. *ACS Catal.* **11**, 12532–12542.
  46. Diment, W.T., and Williams, C.K. (2022). Chain end-group selectivity using an organometallic

- Al(III)/K(I) ring-opening copolymerization catalyst delivers high molar mass, monodisperse polyesters. *Chem. Sci.* **13**, 8543–8549.
47. C. Fornaçon-Wood, C. Gallizioli, M. Stühler, P. Pröhm, C. Müller, A. J. Plajer. (2023) ChemRxiv. Cooperative taming of CS<sub>2</sub>/oxetane copolymerisation: Consequences of main-chain sulfuration on polymer properties and catalysis. <https://doi.org/10.26434/chemrxiv-2023-8hjqs2>.
48. Deacy, A.C., Phanopoulos, A., Lindeboom, W., Buchard, A., and Williams, C.K. (2022). Insights into the Mechanism of Carbon Dioxide and Propylene Oxide Ring-Opening Copolymerization Using a Co(III)/K(I) Heterodinuclear Catalyst. *J. Am. Chem. Soc.* **144**, 17929–17938.
49. Li, Z., Mayer, R.J., Ofial, A.R., and Mayr, H. (2020). From Carbodiimides to Carbon Dioxide: Quantification of the Electrophilic Reactivities of Heteroallenes. *J. Am. Chem. Soc.* **142**, 8383–8402.
50. Xu, J., Zhang, P., Yuan, Y., and Hadjichristidis, N. (2023). Elucidation of the alternating copolymerization mechanism of epoxides or aziridines with cyclic anhydrides in the presence of halide salts. *Angew. Chem. Int. Ed.* **62**, e202218891. <https://doi.org/10.1002/anie.202218891>.
51. Yang, J.-L., Wang, Y., Cao, X.-H., Zhang, C.-J., Chen, Z., and Zhang, X.-H. (2021). Enabling Oxygen–Sulfur Exchange Reaction to Produce Semicrystalline Copolymers from Carbon Disulfide and Ethylene Oxide. *Macromol. Rapid Commun.* **42**, 2000472.
52. Hardy, C., Kociok-Köhn, G., and Buchard, A. (2022). UV degradation of poly(lactic acid) materials through copolymerisation with a sugar-derived cyclic xanthate. *Chem. Commun.* **58**, 5463–5466.